Astronomy & Astrophysics

Photoionization models for extreme Lyα λ1216 and HeII λ1640 ratios in quasar halos, and PopIII vs. AGN diagnostics

A. Humphrey[1], M. Villar-Martín[2], L. Binette[3], and R. Raj[1,4]

[1] Instituto de Astrofísica e Ciências do Espaço, Universidade do Porto, CAUP, Rua das Estrelas, 4150-762 Porto, Portugal
    e-mail: andrew.humphrey@astro.up.pt
[2] Centro de Astrobiología (INTA-CSIC), Ctra de Torrejón a Ajalvir, km 4, 28850 Torrejón de Ardoz, Madrid, Spain
[3] Instituto de Astronomía, Universidad Nacional Autónomo de México, Ap. 70-264, DF 04510 México, Mexico
[4] Indian Institute of Technology Guwahati, Guwahati 781039, India

ABSTRACT

Aims. We explore potential mechanisms to produce extremely high Lyα/HeII flux ratios, or to enhance the observed number of Lyα photons per incident ionizing photon, in extended active galactic nucleus (AGN) photoionized nebulae at high-redshift.
Methods. We computed models to simulate, in the low density regime, photoionization of interstellar gas by the radiation field of a luminous AGN. We have explored the impact of ionization parameter, gas metallicity, ionizing spectrum, electron energy distribution, and cloud viewing angle on the relative fluxes of Lyα, HeII and other lines, and on the observed number of Lyα photons per incident ionizing photon. We have compared our model results with recent observations of quasar Lyα halos at $z \sim 3.5$.
Results. Low ionization parameter, a relatively soft or filtered ionizing spectrum, low gas metallicity, κ-distributed electron energies, or reflection of Lyα photons by neutral hydrogen can all result in significantly enhanced Lyα relative to other lines ($\geq$10%), with log Lyα/HeII reaching values of up to 4.6. In the cases of low gas metallicity, reflection by HI, or a hard or filtered ionizing spectrum, the observed number of Lyα photons per incident ionizing photon is itself significantly enhanced above the nominal Case B value of 0.66 due to collisional excitation, reaching values as high as 5.3 in an "extreme case" model which combines several of these effects. We find that at low gas metallicity (e.g. $Z/Z_\odot = 0.1$) the production of Lyα photons is predominantly via collisional excitation rather than by recombination. In addition, we find that the collisional excitation of Lyα becomes much more efficient if the ionizing continuum spectrum has been pre-filtered through an optically thin screen of gas closer to the AGN (e.g. by a wide-angle, feedback-driven outflow). We also show that the Lyα and HeII emission line ratios of a sample of previously studied quasars at $z \sim 3.5$ are consistent with AGN-photoionization of gas with moderate to low metallicity and/or low ionization parameter, without requiring exotic ionization or excitation mechanisms such as strong line-transfer effects. In addition, we present a set of UV-optical diagnostic diagrams to distinguish between photoionization by Pop III stars and photoionization by an AGN.

Key words. galaxies: high-redshift – galaxies: abundances – galaxies: active – galaxies: ISM – quasars: emission lines – galaxies: halos

1. Introduction

The Lyman-alpha (Lyα λ1216) line of neutral hydrogen is an important observable in that it permits the discovery and study of galaxies at high redshift (e.g. Shibuya et al. 2018), particularly galaxies in a phase of star formation or active galactic nucleus (AGN) activity. This line is one of the intrinsically most luminous in galaxy spectra, but is relatively unstable as a quantitative diagnostic due to its resonant nature, and also due to its susceptibility to extinction by dust or other effects (e.g. Binette et al. 1993a). Despite its significant disadvantages, Lyα remains a key source of observational information about the evolution of galaxies and their gaseous environments across cosmic time (e.g. Haiman & Rees 2001).

Although typically less luminous and thus more difficult to observe, the non-resonant recombination line HeII λ1640 offers additional information to that provided by Lyα. Crucially, the ionization potential of He$^+$ is far higher than that of H^0 (54.4 vs. 13.6 eV) and the production of a significant flux of HeII relative to Lyα requires an ionizing source with a relatively hard ionizing spectrum, or else significant collisional ionization by shocks. Used together, Lyα and HeII offer potentially powerful

diagnostics of the nature of ionizing sources in high-z galaxies, and a toolbox for understanding the physics of gaseous nebulae therein (e.g. Heckman et al. 1991; Villar-Martín et al. 2007; Arrigoni Battaia et al. 2015a; Feltre et al. 2016; Husemann et al. 2018; Dors et al. 2018).

One potentially powerful application of the Lyα to HeII flux ratio is in the identification of Population III (Pop III) stars in the high redshift Universe, by searching for HII regions or star forming galaxies with an emission line spectrum indicative of photoionization by an extremely hot thermal source (e.g. Schaerer 2002). However, care is needed to avoid misclassifying AGN as Pop III and vice versa (see e.g. Fosbury et al. 2003; Binette et al. 2003; Villar-Martín et al. 2004; Sobral et al. 2015, 2019; Bowler et al. 2016).

In addition, the Lyα to HeII flux ratio can inform us about the physics in nebulae associated with powerful AGN. For example, transfer effects and dust can strongly affect this line ratio (e.g. van Ojik et al. 1994; Villar-Martín et al. 1996), and photoionization modelling also suggests that the gas density and metallicity and the presence of young stars may also impact this line ratio in nebulae that are photoionized by an AGN (Villar-Martín et al. 2007).

Building on previous modelling (e.g. Villar-Martín et al. 1996, 2007; Arrigoni Battaia et al. 2015a,b), we present photoionization model calculations appropriate for large-scale Lyα nebulae photoionized by an AGN. In particular, we explore several potential mechanisms to produce "extreme" Lyα and HeII emission line ratios, or an enhancement in the number of Lyα photons per incident ionizing photon. In addition, we explore possible diagnostic diagrams to distinguish between photoionization by an AGN and photoionization by PopIII-like stars.

2. Defining "extreme" Lyα flux ratios

This study was motivated in part by the recent discovery by Borisova et al. (2016) of Lyα halos around a number of quasars at $z \sim 3.5$, with Lyα $\lambda1216$/HeII $\lambda1640$ flux ratios that are typically significantly higher than those measured from the spatially integrated spectra of powerful radio galaxies at $z>2$ (e.g. Vernet et al. 2001; Villar-Martín et al. 2007). Following Villar-Martín et al. 2007, we consider Lyα/HeII $\lambda1640 > 15$ (1.18 in log) to be an "extreme" ratio. This is above the normal range of values shown by high-z radio galaxies (see also De Breuck et al. 2000; Vernet et al. 2001), and above the range of values produced by ionization-bounded photoionization models that are able to reproduce the UV line ratios of $z \sim 2$ radio galaxies (see, e.g. Villar-Martín et al. 1997, 2007).

3. Photoionization modelling

In order to examine how various physical conditions and the nature of the ionizing source can affect the emergent emission line spectrum of a photoionized nebula, we have computed a grid of photoionization models using the multi-purpose modelling code MAPPINGS 1e (Binette et al. 1985, 2012; Ferruit et al. 1997). Some regions of parameter space we investigate here have also been explored previously (e.g. Villar-Martín et al. 1996, 2007; Arrigoni Battaia et al. 2015a,b). Here we build on existing work by considering a wider range of parameter space, additional parameters, and previously unexplored combinations of parameters. Two-photon emission is present in all our models, due to the modelled plasma being in the low-density regime.

3.1. Fixed parameters

We keep several model parameters fixed throughout this study. For simplicity, we adopt an isochoric, plane-parallel, single-slab geometry. By default, the models are ionization-bounded unless otherwise stated, with computation terminated when the ionization fraction of hydrogen falls below 0.01.

3.2. Gas density n_H

Throughout this paper, we define n_H as the Hydrogen gas number density within our line emission models. Thus, all values of n_H discussed herein are not necessarily directly equivalent to the volume-averaged gas densities which are often preferred when modelling large scale structure (e.g. Rosdahl & Blaizot 2012).

We have adopted $100 \, \text{cm}^{-3}$ as our default hydrogen number density, because we aim to simulate spatially extended, low density gas rather than compact regions of high density gas closely associated with the central AGN, whose gas clouds typically have $n_H > 1000 \, \text{cm}^{-3}$. To test the impact of lower gas density on the Lyα emission, we have computed additional models using $n_H = 0.1 \, \text{cm}^{-3}$, corresponding to the volume-averaged gas density in the outskirts of high-z quasar halos predicted by the numerical simulations of Rosdahl & Blaizot (2012).

3.3. Ionization parameter U

The ionization parameter[1] U is effectively a measure of the ratio of ionizing photons to particles in the model gas cloud, and provides a useful parameterization of the ionization state of the gas. High-z Lyα emitters can be very large ($r > 100$ kpc), and there is a potentially very large range in U between individual objects and between different regions of objects, depending on r, Q, n_H, etc. For example, a cloud of gas in the outer Lyα halo of a luminous quasar might have log $U \sim -3.5$ (assuming $Q \sim 10^{56} \, \text{s}^{-1}$, $r \sim 100$ kpc, $n_H \sim 10 \, \text{cm}^{-3}$). A cloud closer to the quasar for instance might have log $U \sim -1.5$ (with $r \sim 1$ kpc, $n_H \sim 1000 \, \text{cm}^{-3}$). On the other hand, a cloud might have log $U \sim -4.5$ with $n_H \sim 1 \, \text{cm}^{-3}$ at a distance of $r \sim 1$ Mpc from a quasar. Thus, we should consider a suitably large range in U. Our model grid contains 100 values of U, starting at log $U = -5$ and ending at log $U = 0.25$. We increase U by +0.0531 dex (i.e., a factor of 1.13) between each model in the U-sequence to obtain a relatively fine sampling of this parameter.

3.4. Ionizing powerlaw index

By default, we adopt a power law with the canonical spectral index $\alpha = -1.5$ (e.g. Robinson et al. 1987), where $S_\nu \propto \nu^{+\alpha}$ (see also Telfer et al. 2002; Shull et al. 2012; Stevans et al. 2014). However, it has been suggested that AGN at high redshift (i.e., $z \gtrsim 2$) have a significantly harder ionizing spectrum (e.g. Francis 1993; Villar-Martín et al. 1997). On the other hand, it is conceivable that some active galaxies at high redshifts may instead have softer ionizing SEDs, due to the presence of a massive starburst which could contribute photons to the ionization of the extended Lyα halo (e.g. Villar-Martín et al. 2007), or perhaps due to partial filtering of the AGN's ionizing continuum in a circumnuclear screen of gas (e.g. Binette et al. 2003). To test the impact of adopting a harder or softer powerlaw, we have also computed model sequences using $\alpha = -1.0$ or $\alpha = -2.0$.

3.5. Gas chemical abundances

We also vary the gas chemical abundances, to examine the impact of metallicity on the emergent emission line spectrum. As the starting point for the chemical abundance sets considered here, we adopt the Solar chemical abundances as determined by Asplund et al. (2006). For non-Solar gas abundances, we scale all metals linearly.

Lyα emitting regions associated with galaxies at high-z have a potentially very large dispersion in gas metallicity, ranging from extremely metal poor gas on the outskirts of a very young galaxy at high redshift, to metal-enriched gas close to the active nucleus of a massive galaxy. Thus, we consider three representative gas metallicities of $Z = 0.01, 0.10$, and 1.0 times the Solar metallicity ($Z_\odot$).

3.6. Electron energy distribution and κ

Among the novel features of MAPPINGS 1e is the ability to use the non-equilibrium, Kappa-distribution (KD) of electron energies instead of the commonly adopted Maxwell–Boltzmann distribution (MBD). The KD of electron energies used in MAPPINGS 1e is a function of electron temperature and the κ

---

[1] $U = \frac{Q}{4\pi r^2 c n_H}$, where Q is the luminosity of ionizing photons emitted by the ionizing source assuming it is isotropic, r is the distance of the cloud from the ionizing source, and n_H is the hydrogen density of the cloud.

parameter, where $1.5 < \kappa < \infty$, and is described in Nicholls et al. (2012; see also Vasyliunas 1968). When $\kappa \to \infty$, the distribution becomes a MBD. Full details of the implementation of KD electron energies in MAPPINGS 1e are given in Binette et al. (2012).

Although the physics underpinning the KD is not yet fully understood (see, e.g. Ferland et al. 2016; Draine & Kreisch 2018), the presence of KD energies in Solar System plasmas is well established (e.g. Vasyliunas 1968; Livadiotis & McComas 2011; Livadiotis 2018). Thus, it is important to consider the possibility that KD electron energies may be present in some extrasolar and extragalactic plasmas. Indeed, a number of recent studies have shown that many commonly observed nebular emission lines can be significantly affected by adopting the KD, both in HII regions and high-z radio galaxies, and the KD has been proposed as a solution to the long-standing observational temperature discrepancies in planetary nebulae and HII regions (Nicholls et al. 2012, 2013; Binette et al. 2012; Humphrey & Binette 2014).

Values in the range $10 \lesssim \kappa \lesssim 40$ have been proposed for HII regions and planetary nebulae (e.g. Nicholls et al. 2012; Binette et al. 2012) and AGN (Humphrey & Binette 2014), where a smaller κ represents a stronger deviation from the MBD. In this Paper we consider $\kappa = 20$ in place of the MBD distribution in some model sequences.

3.7. Cloud viewing angle

As previously shown by Villar-Martín et al. (1996), neutral hydrogen at the back of the cloud can act as a "mirror" to backscatter Lyα towards the front of the cloud, enhancing the flux of Lyα as seen by the observer, relative to other lines. To avoid confusion with other geometrical set-ups, we refer to this neutral "mirror" at the rear of the cloud as a "back-mirror".

We consider two viewing angles for the model cloud (slab). By default, we have adopted the "side view", which places the observer at an angle of $90°$ to the direction of travel of the incident ionizing radiation. In addition, we also calculate the "front view", where the observer views the illuminated face of the cloud (see Binette et al. 1993a,b). In all of our ionization-bounded models, the column density of neutral hydrogen towards the back of the cloud ($N_{HI} \geq 10^{18}$ cm^{-2}) is substantially higher than what is required to produce a significant neutral "back-mirror" effect (the minimum required is $N_{HI} \gtrsim 10^{14}$ cm^{-2}). This "back-mirror" effect would be much weaker in models in which the illuminated gas is optically thin to ionizing radiation (matter-bounded), such as the filtering screen described in Sect. 3.8 below, or the optically thin photoionization models that Arrigoni Battaia et al. (2015b) favoured in explaining the Lyα emission from the giant gas halo of the $z = 2.28$ quasar UM287.

To reflect Lyα photons from the active nucleus (whether hidden or viewed directly), such neutral "back-mirrors" as considered here are not strictly needed. This is because even a matter-bounded HII slab of reasonable opacity (e.g. Binette et al. 1996) will have a non-negligible HI fraction and thus can scatter to our line-of-sight Lyα photons from the active nucleus (e.g. Humphrey et al. 2013a; Cantalupo et al. 2014), potentially providing a further enhancement to the flux of Lyα. However, we do not consider this additional effect here.

3.8. Ionization by a filtered SED

We also study the impact of photoionizing gas clouds using an ionizing powerlaw SED that has first been filtered through a screen of gas that does not fully absorb all ionizing photons. A situation where this might occur would be in a galaxy which contains a wind-blown superbubble that is expanding into the extended gaseous halo (e.g. Tenorio-Tagle et al. 1999; Taniguchi et al. 2001). In this case, one would expect the bubble to partially filter the AGN's ionizing continuum so that gas clouds at radii beyond the bubble would see an altered version of the ionizing SED. Alternatively, the ionizing spectrum of the AGN might be filtered by gas in the host galaxy, before escaping to ionize gas on hundreds of kpc scales, giving essentially the same result. Several previous studies have addressed this issue (see e.g. Binette et al. 1996, 2003), and among the main effects are lower fluxes for HeII and other high-ionization lines, and lower electron temperatures, than would have resulted using the original (unfiltered) SED.

Here, we look specifically at the impact of a filtered ionizing SED on Lyα flux ratios. For this, we have produced a set of four filtered SEDs by computing matter-bounded photoionization models with $\alpha = -1.5$, $\log U = -2$ and $N_H = 1.0, 2.5, 5.0$ or 7.0×10^{20} cm^{-2}, giving ionizing continuum escape fractions of $F_{esc} = 0.90, 0.74, 0.50$ and 0.28, respectively[2]. The choice of values for U and N_H are not critical, and can be scaled in lockstep to produce a similar emergent distribution. The metallicity of the screening gas is assumed to be solar. The resulting ionizing SEDs were then used as inputs for new, U-sequence model calculations.

The various filtered SEDs are shown in Fig. 1. The main dips seen in our filtered SEDs are caused by photoelectric absorption of photons by H (13.6 eV) and He$^+$ (54.4 eV), resulting in a spectrum with a comparatively lower number of He$^+$ ionizing photons. For comparison, we also show the residual of an $\alpha = -1.5$ ionizing SED from an unfiltered model calculation.

When computing models using a filtered SED, we have scaled by F_{esc} the range in U values covered. For instance, when using our $F_{esc} = 0.28$ SED, our U-sequences run from $\log U = -4.55$ to $\log U = -0.30$. This introduces a differential shift in the curves that are plotted as a function of U. To facilitate visual comparison between models, we show in Appendix A the same models as a function of $U_* = U/F_{esc}$.

We do not include line emission produced within the filtering screen in the resulting line fluxes from our filtered continuum models. The relative significance of the line flux from the absorbing screen depends strongly on its physical conditions, and can varies from significant when the screen and post-screen gases have similar physical conditions (see the models of Binette et al. 1996), to negligible as in the case where the filtering screen is obscured (from the observer) by nuclear dust. A full treatment of the emission from such a screen is beyond the scope of this paper.

3.9. Ionization by Pop III stars

We also include a model sequence to simulate a low-metallicity nebula being photoionized by Pop III (or Pop III-like) stars, with the aim of understanding to what extent their Lyα flux ratios differ from those of our AGN models. Taking into account the effect of He$^+$ opacity, a zero-metallicity star with an effective temperature of 80 000 K would be equivalent to a black-body of 67 200 K in terms of the proportion of He$^+$-ionizing photons (see Holden et al. 2001; Schaerer 2002; Binette et al. 2003). Thus, we adopt a black-body temperature of 67 200 K in this model sequence.

---

[2] We define F_{esc} as the fraction of H-ionizing photons that pass through the filtering screen of gas unabsorbed.
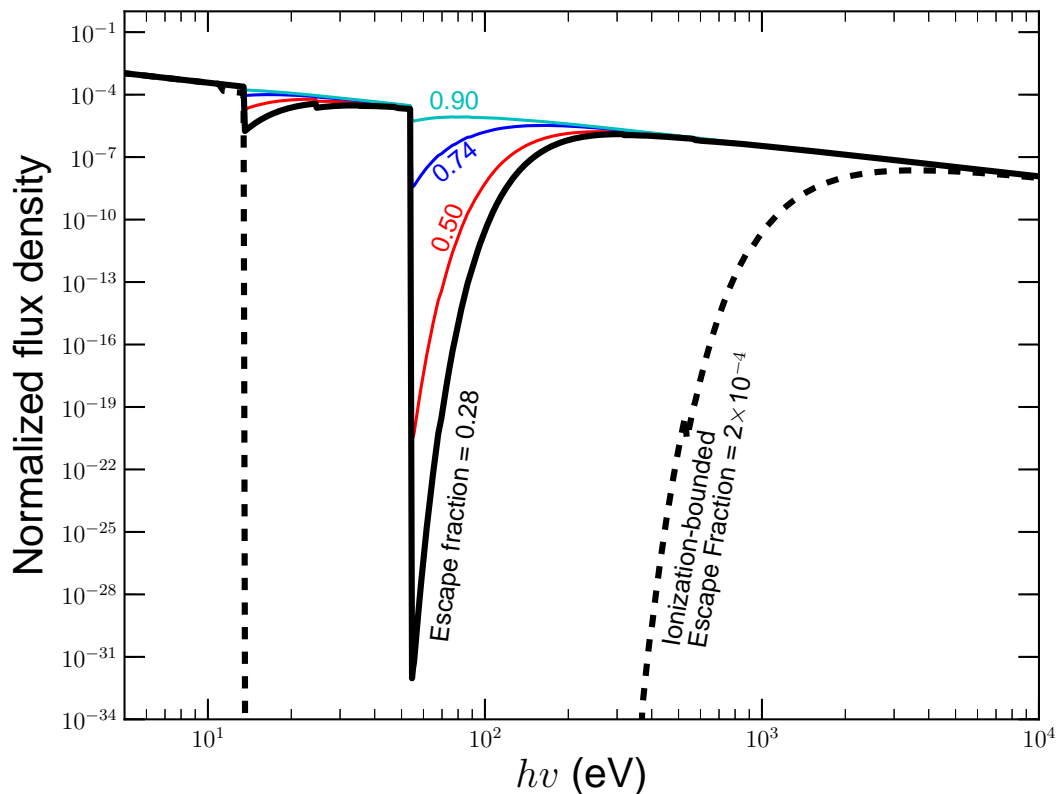
Fig. 1. Filtered AGN spectral energy distributions described in Sect. 3.8. These correspond to escape fractions of 0.28 (solid black line), 0.50 (solid red line), 0.74 (solid blue line) and 0.90 (solid cyan line). For comparison, we also show the emergent distribution from a typical ionization-bounded model (dashed black line): the UV part of the spectrum has been completely absorbed, while some X-rays still escape through the cloud. The vertical axis (normalized flux density or S_ν) gives the power per unit area per unit frequency in arbitrary units. The escape fractions are in photon number flux, while the SEDs are plotted in energy flux per unit frequency (S_ν).

We also use a gas phase metallicity of $Z/Z_\odot = 0.01$, to account for some slight pollution with metals, and for consistency with the low-metallicity AGN powerlaw models against which our Pop III models will be compared. For easy comparison with our AGN models, our Pop III models use an ionization-bounded, plane-parallel geometry and $n_{\rm H} = 100\,{\rm cm}^{-3}$.

It is not our intention to model in detail the expected line spectrum of a Pop III-ionized nebula, but to reach a general overview of the potential for such a nebula to be confused with an AGN-photoionized nebula when only the strongest UV emission lines are available. We stress that this model sequence may be unrealistic in that true Pop III stars are expected to form from chemically primordial gas, with the associated HII region being similarly devoid of metals. Our model sequence, however, does consider a zero-metallicity Pop III star (or stars), but the gas it photoionizes has already undergone some slight polution with metals. In a future paper we will present a more detailed modelling of emission line diagnostics for Pop III HII-regions and Pop III galaxies.

4. Results

Here we describe the results from our model grid using diagnostic diagrams, which we show in Figs. 2–7.

4.1. AGN models – line ratios

Our modelling shows that "extreme" ratios of Lyα/HeII can be readily produced using AGN photoionization. Within our model grid this flux ratio spans a huge range in values, from log Lyα/HeII ~1.1 to ~4.6, without the need to invoke physically implausible values for model parameters. Below we describe the impact of individual parameters on the line ratios, giving examples to quantify the impact at specific positions within our parameter space.

We find that Lyα/HeII is extremely high when U is relatively low, regardless of which electron energy distribution and gas metallicity are selected, as can be seen in Fig. 2. For example, at $Z/Z_\odot = 0.1$ and log $U = -4$ we obtain log Lyα/HeII = 1.88. There is essentially no upper limit to the Lyα/HeII flux ratio, with Lyα/HeII $\to \infty$ as $U \to 0$ (log $U \to -\infty$). We also note that most of the model sequences show at their high-U end (log $U \gtrsim -2.5$) a region of relatively constant Lyα/HeII values, confirming that this ratio is relatively insensitive to U in the high-ionization regime (Fig. 2; see also e.g. Villar-Martín et al. 2007; Arrigoni Battaia et al. 2015b).

As shown by previous authors, a reduction in gas metallicity results in enhanced emission of Lyα relative to HeII due to increased collisional excitation of Lyα resulting from the increase in electron temperature (e.g. Villar-Martín et al. 2007). As shown in Fig. 2, our models indicate that this effect can also strongly enhance Lyα/Hβ. On the other hand, Hα/Hβ and Lyα/Hα show relatively small increases with reducing metallicity. For instance, when log $U = -2$ and $\alpha = -1.5$, moving from $Z/Z_\odot = 1.0$ to $Z/Z_\odot = 0.1$ changes log Lyα/HeII from 1.25 to 1.46 (+0.21 dex); log Lyα/Hβ from 1.43 to 1.59 (+0.16 dex); Lyα/Hα from 0.96 to 1.10 (+0.14 dex); Hα/Hβ from 0.46 to 0.49 (+0.03 dex).
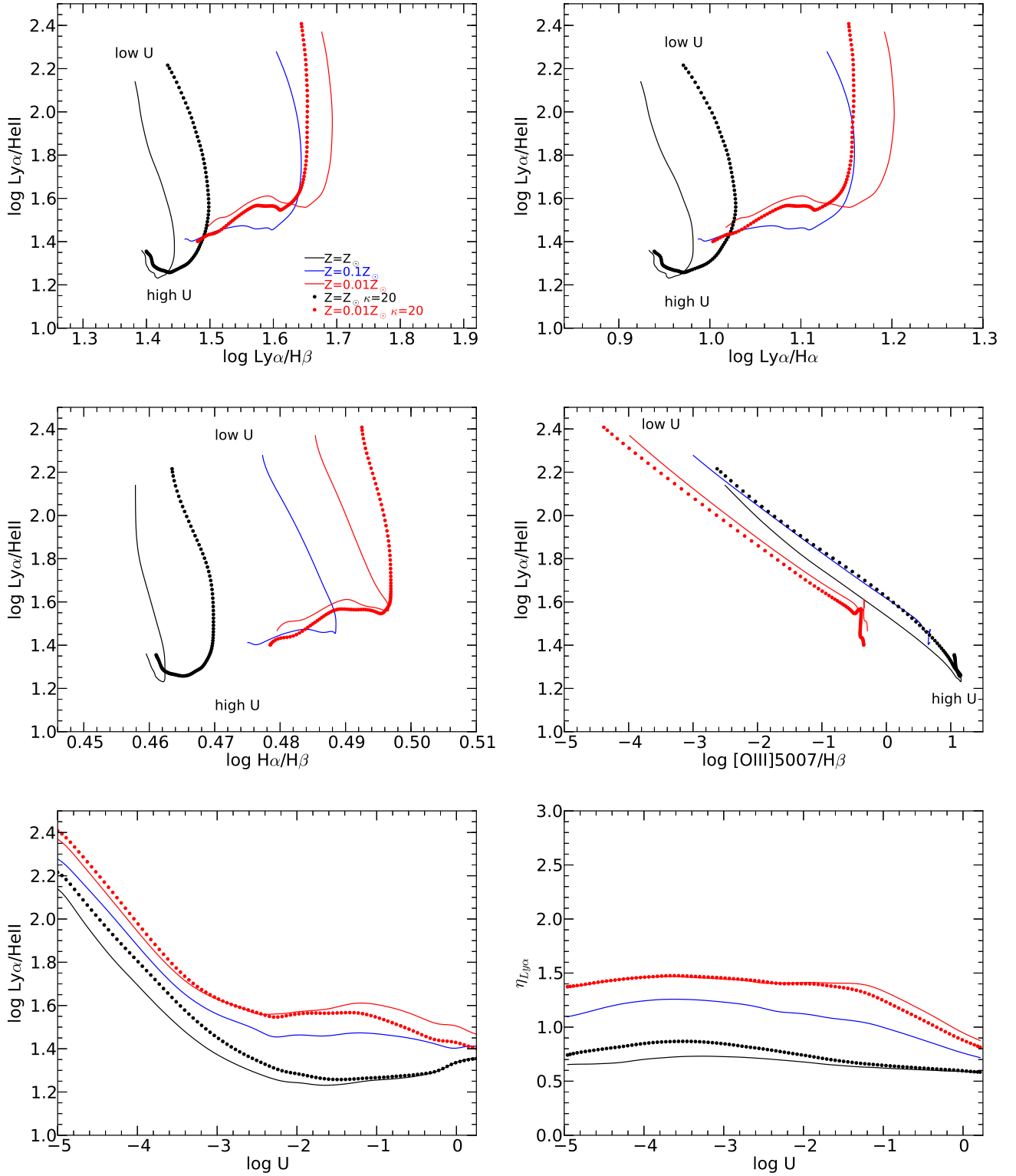
Fig. 2. Selected sequences in U plotted for Lyα/HeII vs. Lyα/Hβ, Lyα/Hα, Hα/Hβ, or [OIII] $\lambda5007$/Hβ. Each sequence represents a progression in U, for each of the three values of Z. Also shown are sequences in U using $\kappa = 20$ for $Z/Z_\odot = 0.01$ and 1.0 (dotted curves). All models in this figure use power index $\alpha = -1.5$. *The lower two panels* show Lyα/HeII vs. U (*left*) and the ratio of Lyα photons to ionizing photons ($\eta_{Ly\alpha}$; *right*) for the same model sequences. The model loci cover the range of ionization parameter $-5 < \log U < 0.25$.

The impact of using the κ-distribution is complex and varies across the range in parameter space we examine in this work. Generally speaking, using $\kappa = 20$ results in a minor enhancement of Lyα relative to HeII, Hβ and Hα at high metallicity ($Z/Z_\odot \gtrsim 1.0$), but when metallicity is low ($Z/Z_\odot \lesssim 0.1$) the

Lyα is marginally reduced relative to those lines. For instance, at $\log U = -2$, $\alpha = -1.5$ and $Z/Z_\odot \gtrsim 1.0$, $\log$ Lyα/Hβ changes from 1.43 to 1.46 (+0.03 dex) when adopting $\kappa = 20$, but at $Z/Z_\odot \gtrsim 0.1$ we find that using $\kappa = 20$ reduces $\log$ Lyα/Hβ from 1.59 to 1.58 (−0.01 dex). In other words, the impact on Lyα of
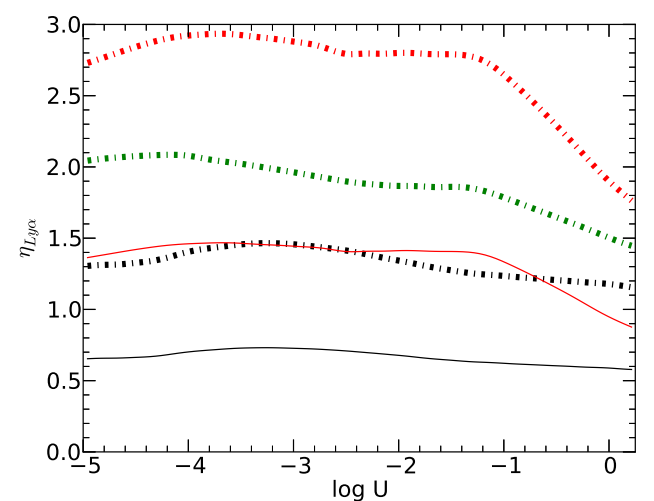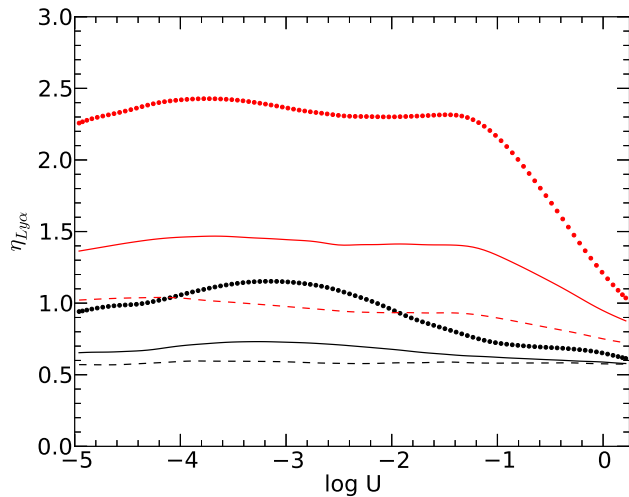
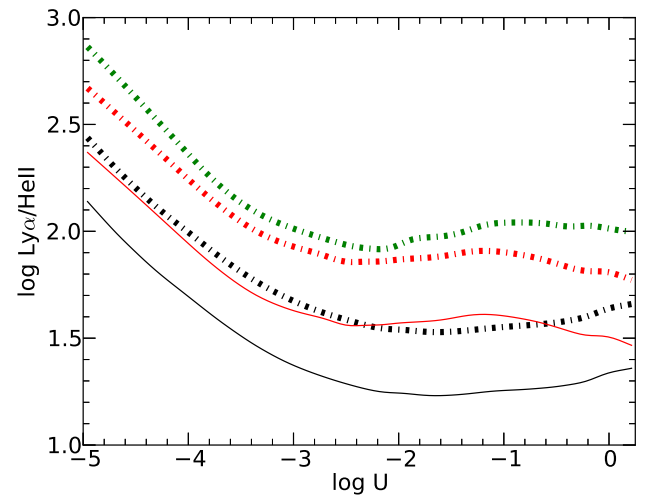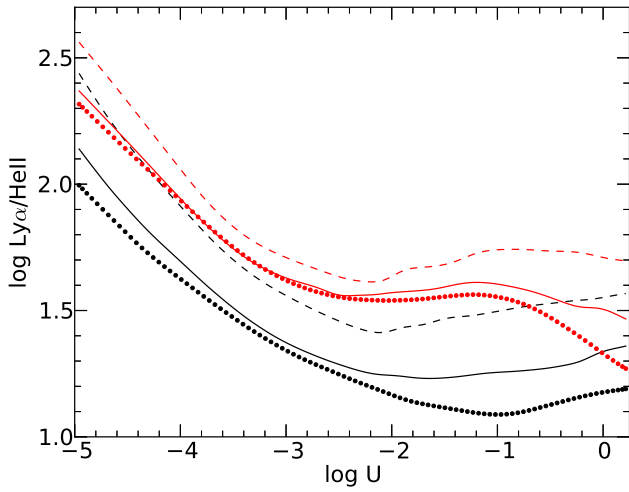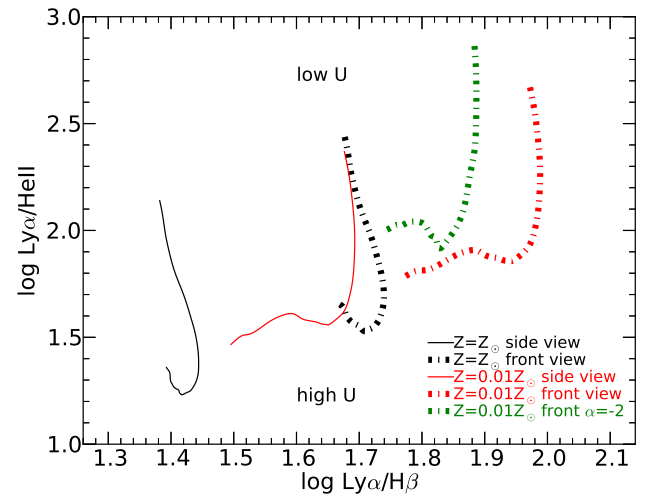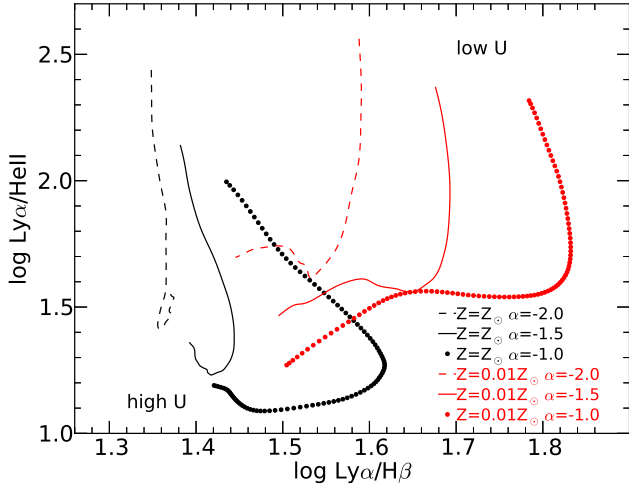**Fig. 3.** Impact of the powerlaw index of the ionizing spectrum on Lyα/HeII, Lyα/Hβ and $\eta_{Ly\alpha}$. The model loci cover the range of ionization parameter $-5 < \log U < 0.25$.

Fig. 4. Impact of viewing angle on the observed Lyα/HeII, Lyα/Hβ and $\eta_{Ly\alpha}$ values. The green curve shows the locus of our sequence in U using $Z/Z_{\odot} = 0.01$, $\alpha = -2.0$ and the "front view", to illustrate the combined effect of low U, low gas metallicity, a relatively soft ionizing continuum, and a "back-mirror". The model loci cover the range of ionization parameter $-5 < \log U < 0.25$.

adopting a κ-distribution with $\kappa = 20$ is marginal to insignificant, at least in the range of parameter space we consider herein. A full analysis of the impact of using the KD in place of the MBD on the emergent spectrum of active galaxies and high-z Lyα emitters will be presented in a future Paper (Morais et al., in prep.).

Figure 3 shows the impact of using different ionizing spectral indices (α). As expected from previous studies (e.g. Humphrey et al. 2008; Arrigoni Battaia et al. 2015b), the Lyα/HeII flux ratio is higher when using a softer ionizing
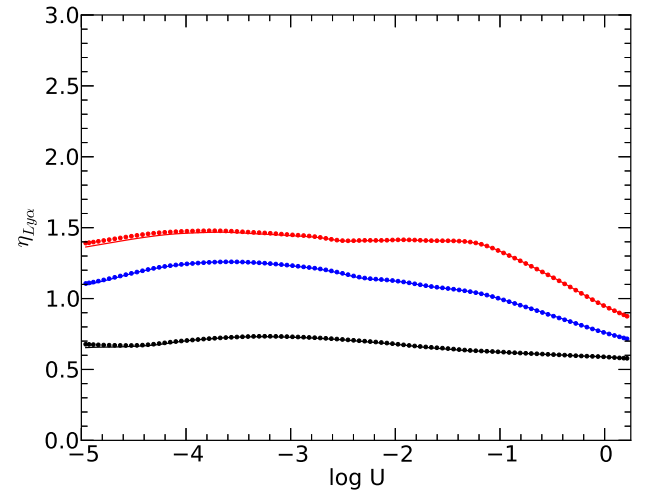
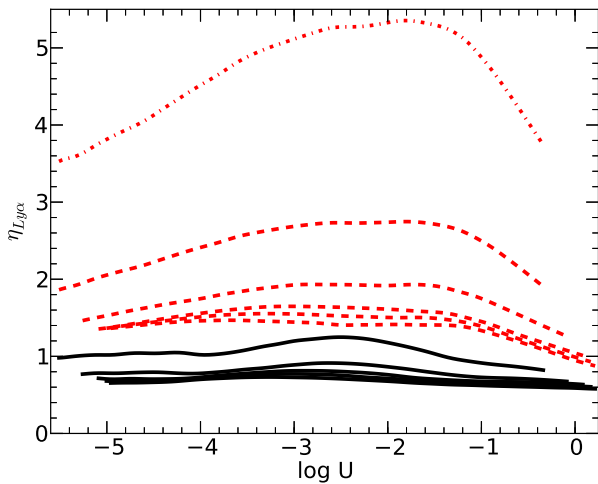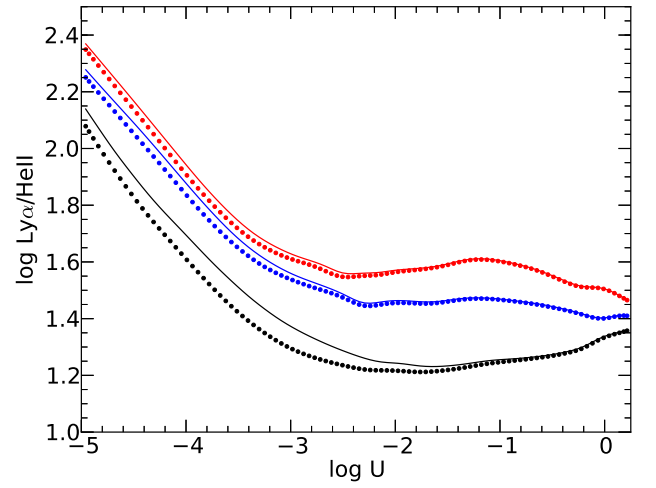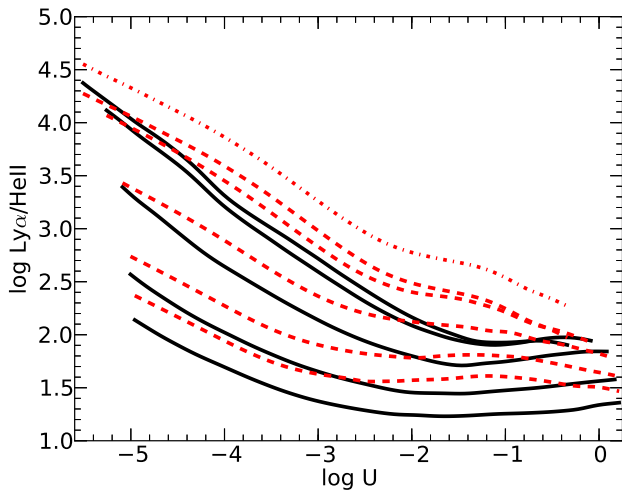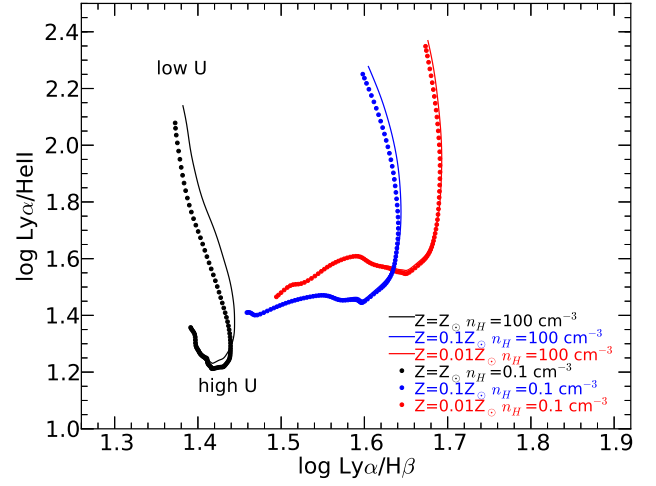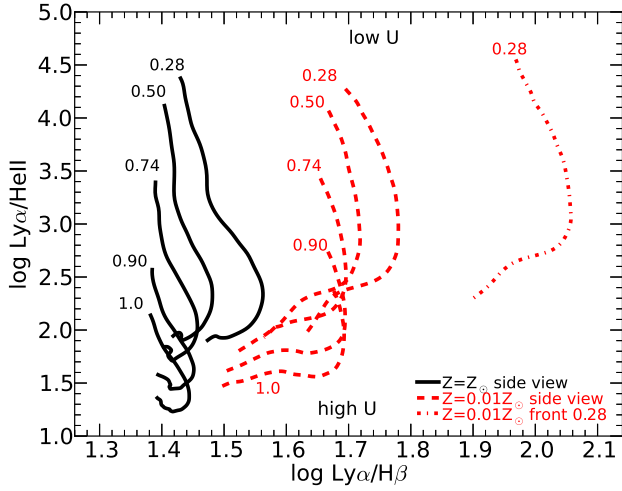**Fig. 5.** Impact of using a filtered ionizing continuum instead of a simple powerlaw on the observed values of Lyα/HeII, Lyα/Hβ and $\eta_{Ly\alpha}$. U-sequences using a filtered ionizing continuum are labelled with their value of F_{esc}. U-sequence loci which use our default powerlaw of $\alpha = -1.5$ are labelled "1.0" because the input SED is unfiltered. The dot-dashed curve (on the right of the *upper panel*) shows the locus of our sequence in U that uses $F_{esc} = 0.28$, $Z/Z_\odot = 0.01$, $\alpha = -1.5$ and the "front view", to illustrate the combined effect of low U, low gas metallicity, a heavily filtered ionizing continuum, and a "back-mirror". For each combination of U and $Z/Z_\odot$, a lower F_{esc} results in lower Lyα/HeII and higher $\eta_{Ly\alpha}$. In Fig. A.1 we show an alternate version of this Figure, plotted with U scaled by $1/F_{esc}$ to aid comparison with our other models.

Fig. 6. Impact of gas density on the observed Lyα/HeII, Lyα/Hβ and $\eta_{Ly\alpha}$ values. The model loci cover the range of ionization parameter $-5 < \log U < 0.25$.

spectrum, because there are relatively fewer photons able to ionize He$^+$ ($h\nu > 54.4$ eV). However, a softer ionizing SED results in a reduction in the flux of Lyα relative to Hβ and Hα, and a reduction in Hα/Hβ, because a softer SED results in lower electron temperatures, reducing the importance of collisional excitation effects on these lines. For instance, at $\log U = -2$ and $Z/Z_\odot$,

we find that moving from $\alpha = -1.0$ to $\alpha = -2.0$ changes log Lyα/HeII from 1.17 to 1.44 (+0.27 dex), log Lyα/Hβ from 1.59 to 1.37 (−0.22 dex), log Lyα/Hα from 1.11 to 0.91 (−0.20 dex), log Hα/Hβ from 0.48 (3.04) to 0.45 (2.84), and $< T_{\rm OIII} >$ from 14700 K to 9200 K.

In Fig. 4 we show the effect of adopting the "front view" in our adopted geometry. In our models, the observed flux of Lyα (relative to other lines) is nearly twice that of the "side view", with HI in the partially ionized or neutral zone reflecting almost all of the incident Lyα emission, close to the factor 2.0 (0.3 dex) theoretical maximum effect for a uniformly flat "back-mirror" with a covering factor of unity. Interestingly, Fig. 4 also reveals a degeneracy between metallicity and cloud viewing angle, with the "front view" mimicking models that use the "side view" with a lower gas metallicity. Conversely, "rear view" models (not shown) result in much lower Lyα flux relative to most other lines, as there is no direct Lyα.

As expected, using a filtered ionizing SED results in an enhancement of Lyα/HeII compared to the original, unfiltered SED (Fig. 5). This is primarily because the absorbing screen preferentially absorbs photons in the range 54.4–200 eV, reducing the relative number of photons that can ionize He$^+$ ($h\nu \geq$ 54.4 eV) compared to H (see Fig. 1). The enhancement in Lyα/HeII is also partly due to increased collisional excitation of Lyα (see discussion of $\eta_{\rm Ly\alpha}$ in Sect. 4.2), via two different effects: (i) Collisional excitation of Lyα requires the presence of neutral H; because it is relatively harder than the unabsorbed powerlaw, the filtered SED is less efficient at ionizing H, resulting in a higher H neutral fraction and thus a higher rate of collisional excitation of Lyα; (ii) Photoionization by the filtered (harder) SED produces photoelectrons that are on average more energetic, increasing the heating rate and temperature of the gas, again leading to a higher rate of collisional excitation of Lyα. To corroborate the presence of these effects, we show in Table 1 the Lyα/HeII ratio and its relation to gas metallicity, electron temperature, and choice of SED. Even though using a filtered continuum does not always result in a higher average electron temperature, it does increase the Balmer decrement, indicating the increased importance of collisional excitation.

The impact on Lyα/HeII can be large, even when the filtering screen has a high escape fraction. For example, using our $F_{\rm esc} = 0.90$ SED we obtain a Lyα/HeII ratio that is ∼0.2 dex higher than the unfiltered SED. Even for $F_{\rm esc}$ as high as ∼0.97 (not shown here), this line ratio is still significantly enhanced (+0.04 dex or 10 percent). At the other end of the parameter range, we obtain log Lyα/HeII = 4.4 using the $F_{\rm esc} = 0.28$ SED, $Z/Z_\odot = 1.0$ and log $U = -5$, which rises to 4.6 if we also include the effect of a "back-mirror". Using a filtered SED also results in slight increase in Lyα/Hβ, of up to ∼0.1 dex in the extreme case of our $F_{\rm esc} = 0.28$ SED. We also note that lower ionization lines tend to become stronger relative to high-ionization lines and HeII (see e.g. Binette et al. 2003).

We find that gas density has a small, but potentially significant effect on the ratios Lyα/HeII when log $U \lesssim -2$ and $Z/Z_\odot = 1.0$ (Fig. 6). In this parameter range, Lyα/HeII is up to 0.1 dex higher when using $n_{\rm H} = 100 \, {\rm cm}^{-3}$ as compared to an equivalent $n_{\rm H} = 0.1 \, {\rm cm}^{-3}$ model. However, at higher values of U, or at low gas metallicity ($Z/Z_\odot \leq 0.1$), we find no significant difference in the Lyα/HeII ratio between our $n_{\rm H} = 0.1$ and $n_{\rm H} = 100 \, {\rm cm}^{-3}$ models.

We note that combining several of the above effects can have a cumulative enhancement on the Lyα/HeII ratio. This is clearly evident in Figs. 2–5. For instance, we find that photoionization

at low U (e.g. log $U \lesssim -5$) by a moderately filtered continuum (e.g. $F_{\rm esc} \lesssim 0.5$) can result in very extreme Lyα/HeII flux ratios, with log Lyα/HeII $\gtrsim 4$ (Fig. 5). In another extreme case from our model grid, we see that low gas metallicity ($Z/Z_\odot = 0.01$), a relatively soft SED ($\alpha = -2.0$) and low ionization parameter (log $U = -5$) together result in log Lyα/HeII = 2.88 and log Lyα/Hβ = 1.88 (Fig. 3).

4.2. AGN models – Lyα to ionizing photon ratio

It is also interesting to consider how the luminosity of the Lyα line varies across our grid of models. To simplify the comparison between models we use $\eta_{\rm Ly\alpha}$, the ratio of emergent Lyα photons to incident ionizing photons. Figures 2–5 each include a panel showing $\eta_{\rm Ly\alpha}$ vs. log U. Our fiducial model sequence using $\alpha = -1.5$ and $Z/Z_\odot = 1$ (Fig. 2) produces values of $\eta_{\rm Ly\alpha}$ that are close to the value $\eta_{\rm Ly\alpha} = 0.66$ expected for complete absorption of the incident ionizing spectrum and purely recombination emission from gas which is optically thick in the Lyman line series (Case B; e.g. Gould & Weinberg 1996). However, we find significant variation in $\eta_{\rm Ly\alpha}$ across our model grid, which we describe below.

As shown in Fig. 2 (lower right), the gas metallicity can have a strong effect on $\eta_{\rm Ly\alpha}$, with lower metallicities resulting in higher values of $\eta_{\rm Ly\alpha}$ (see also Table 1). For instance, reducing $Z/Z_\odot$ from 1 to 0.01 increases $\eta_{\rm Ly\alpha}$ by a factor of ∼2. Interestingly, some of our model loci show a substantial drop in $\eta_{\rm Ly\alpha}$ at higher values of U (log $U \gtrsim -2$), particularly in model sequences which use low gas metallicity ($Z/Z_\odot \leq 0.1$) and a hard ionizing SED ($\alpha \geq -1.5$; see, e.g. Fig. 3). Interestingly, when the gas metallicity is sufficiently low ($Z/Z_\odot = 0.01$), the rate of collisional excitation[3] can become the dominant channel for the production of Lyα photons, i.e., at $\eta_{\rm Ly\alpha} \gtrsim 1.4$.

Figure 2 (lower right) also reveals that the choice of electron energy distribution can also have a significant impact on $\eta_{\rm Ly\alpha}$. At high gas metallicity ($Z/Z_\odot = 1$), we find that using $\kappa = 20$ instead of the MBD results in a ∼10–20 percent enhancement of $\eta_{\rm Ly\alpha}$ in the range $-5 < \log U < -2$. However, at low gas metallicity (i.e., $Z/Z_\odot = 0.01$), our κ-distribution models do not show any significant enhancement in $\eta_{\rm Ly\alpha}$, instead showing a ∼10 percent reduction in $\eta_{\rm Ly\alpha}$ at log $U > -1.4$, with no significant difference from the equivalent MBD models when log $U < -1.4$.

The hardness of the ionizing radiation also has an impact on $\eta_{\rm Ly\alpha}$ (Fig. 3), with harder ionizing spectra (higher α) resulting in higher values of $\eta_{\rm Ly\alpha}$. As an example of this, our models with $\alpha = -1.0$ and $Z/Z_\odot = 1$ yield values of $\eta_{\rm Ly\alpha}$ that are up to ∼4 times higher than produced in our $\alpha = -2.0$ $Z/Z_\odot = 1$ models. This difference widens at lower metallicity: at the low-metallicity end of our grid ($Z/Z_\odot = 0.01$), we find that $\eta_{\rm Ly\alpha}$ is a factor of up to ∼30 higher when using $\alpha = -1.0$, compared to $\alpha = -2.0$.

These enhancements of $\eta_{\rm Ly\alpha}$ above the expected Case B value are primarily driven by collisional excitation of Lyα at the enhanced electron temperatures that result from using lower gas metallicity, a harder ionizing spectrum and/or κ-distributed electron energies. The higher neutral H fraction produced by

---

[3] In the low density limit and when the Lyman series is optically thick (Case B), $\eta_{\rm Ly\alpha} \approx \alpha_{2p}^{\rm eff}/\alpha_{\rm B} \approx 0.67(T_{\rm H+}/10^4 \, {\rm K})^{-0.054}$, where α_B is the total recombination coefficient and $\alpha_{2p}^{\rm eff}$ is the effective recombination coeffient for Lyα (see e.g. Binette et al. 1993b). In this regime, values of $\eta_{\rm Ly\alpha} \gtrsim 0.7$ indicate a significant contribution to Lyα production due to collisional excitation, while $\eta_{\rm Ly\alpha} > 1.4$ indicates that collisional excitation is the dominant channel for Lyα production.

Table 1. Illustrating the impact of low gas metallicity and/or a filtered ionizing SED on the production of Lyα.

$Z/Z_\odot$ (1)	$\log U$ (2)	SED (3)	$\langle T_{H^+} \rangle$ (K) (4)	$H^0/(H^0+H^+)$ (5)	H^+/He^{++} (6)	$H\alpha/H\beta$ (7)	Lyα/HeII $\lambda 1640$ (8)	$\eta_{Ly\alpha}$ (9)
1.0	−2	$T = 45\,000$ K	6725	0.053	18705	2.80	5686	0.60
1.0	−2	$\alpha = -1.5$	11605	0.045	48.2	2.90	17.6	0.68
1.0	−2	$F_{esc} = 0.28$	13533	0.120	293.6	3.04	145.2	1.20
0.01	−2	$\alpha = -1.5$	21384	0.054	46.4	3.13	37.0	1.40
0.01	−2	$F_{esc} = 0.28$	20667	0.148	251.3	3.29	304.9	2.80

Notes. Columns are as follows: (1) gas metallicity normalized to the Solar value; (2) log of the ionization parameter U; (3) ionizing SED used (including a black-body SED with $T = 45\,000$ K); (4) average electron temperature in the H^+ zone; (5) hydrogen neutral fraction; (6) ratio of the column density of ionized hydrogen to the column density of fully-ionized helium; (7) Balmer decrement; (8) Lyα to HeII $\lambda 1640$ flux ratio; (9) $\eta_{Ly\alpha}$, the ratio of Lyα photons emitted to incident ionizing photons. The rows have been sorted using $\eta_{Ly\alpha}$. As discussed in the main text, reducing the gas metallicity raises the electron temperature, leading to increased collisional excitation of Lyα (and of Hα relative to Hβ), thus increasing $\eta_{Ly\alpha}$. In addition, adopting a filtered ionizing SED (here we show the $F_{esc} = 0.28$ case) has the dual effect of reducing the abundance of He^{++} relative to H^+ and increasing the collisional excitation of Lyα, with the latter effect resulting in increased $\eta_{Ly\alpha}$.

the filtered SED can also result in a higher rate of collisional excitation of Lyα. As a quantitative illustration of this effect, when using $\alpha = -1.5$ and $\log U = -2$ we find the average electron temperature in the H^+ zone is $T = 11\,605$ K when $Z/Z_\odot = 1$, compared to $T = 21\,383$ K at $Z/Z_\odot = 0.01$, resulting in $\eta_{Ly\alpha} = 0.68$ and $\eta_{Ly\alpha} = 1.40$, respectively (see also Table 1).

In addition, we find that using a filtered ionizing spectrum (Fig. 5) results in an increased $\eta_{Ly\alpha}$, with more strongly filtered spectra producing higher values of $\eta_{Ly\alpha}$. This is primarily due to the increased importance of collisional excitation under such conditions. This effect also results in an increased Balmer decrement (see Table 1).

Although technically not an enhancement in $\eta_{Ly\alpha}$, the inclusion of the effect of a "back-mirror", with the cloud viewed from the front, does also increase the apparent (or observed) $\eta_{Ly\alpha}$ by a factor of ∼2 (Fig. 4). We find no significant difference in $\eta_{Ly\alpha}$ between our $n_H = 0.1$ and $n_H = 100\,\text{cm}^{-3}$ models (Fig. 6).

In summary, we find a substantial variation in $\eta_{Ly\alpha}$, the ratio of Lyα photons to incident ionizing photons, across our AGN photoionization model grid. In particular, there is a substantial deviation from the case B recombination value $\eta_{Ly\alpha} = 0.66$. In our grid, $\eta_{Ly\alpha}$ ranges from a minimum value of $\eta_{Ly\alpha} = 0.58$ in the case of solar metallicity gas illuminated by a powerlaw with $\alpha = -1.5$ at $\log U = 0.25$, to a maximum of $\eta_{Ly\alpha} = 2.7$ for a gas cloud with $Z/Z_\odot = 0.01$ illuminated at $U = -1.6$ by our $F_{esc} = 0.28$ filtered SED. If we also include a neutral "back mirror", then the maximum (effective) value in our grid is $\eta_{Ly\alpha} = 5.3$ (see Fig. 5).

4.3. Degeneracy between AGN and black-body models

Figure 7 shows a comparison between our Pop III U-sequence and AGN U-sequences with the following parameters: (1) $\alpha = -1.5$; (2) $\alpha = -1.5$ with the "front view" of a photoionized slab with a "back-mirror"; (3) $\alpha = -2.0$; (4) photoionization by an $\alpha = -1.5$ powerlaw that has been filtered such that $F_{esc} = 0.50$. All the models use $Z/Z_\odot = 0.01$.

Comparing models with identical values of U, we find that the Pop III models give Lyα/HeII ratios that are around one order of magnitude higher than in the powerlaw AGN models. Nonetheless, three of the AGN sequences do show an overlap in Lyα/HeII with the Pop III sequence. The low-U ends of the $\alpha = -2.0$ and the $\alpha = -1.5$ "front view"

sequences reach up above log Lyα/HeII ∼ 2.5, while the $F_{esc} = 0.50$ filtered continuum model overlaps with the full range of Lyα/HeII values in the Pop III model sequence. In other words, it is not possible to distinguish between photoionization by an AGN or by Pop III stars on the basis of the Lyα/HeII ratio alone[4].

However, the addition of a second line ratio eases the degeneracy between our model sequences. Of the four diagnostic diagrams shown in Fig. 7, the diagram showing Lyα/HeII vs. Lyα/Hβ yields the cleanest separation of models, with the AGN sequences falling below and/or to the right of the Pop III model sequence, because their ionizing SEDs contain a higher proportion of He^+ ionizing photons, and/or because the ionized gas has a higher T_e. This diagram also provides a clear diagnostic to distinguish cases of ionization by a relatively soft source (e.g. Pop-III stars of an $\alpha = -2.0$ powerlaw) from AGN-photoionization by an $\alpha = -1.5$ powerlaw with enhanced Lyα emission due to scattering effects (e.g. our "front view" models). Using a softer ionizing SED shifts a model upwards, while scattering-enhanced Lyα shifts a model up and right.

The other three diagnostic diagrams in Fig. 7 show Lyα/HeII vs. Lyα/CIV $\lambda 1549$, Lyα/CIII] $\lambda\lambda 1907,1909$ and Lyα/CII] $\lambda 2326$. There is a relatively clean separation between the Pop III sequence and the power-law AGN models, which run roughly parallel to each other. Only at their very low-U end do the $\alpha = -2.0$ and "front view" model sequences cross the locus of Pop III models. Interestingly, the filtered AGN continuum sequence crosses the Pop III sequence in all three of our Lyα to carbon diagrams, indicating a degeneracy between these two types of model when Lyα/HeII is used together with ratios involving CIV, CIII] and/or CII] (see also Fosbury et al. 2003; Binette et al. 2003).

5. Discussion

Recently, Borisova et al. (2016) discovered ubiquitous, large-scale Lyα emitting halos around 19 quasars at $z \sim 3.5$. Interestingly, the authors found extreme Lyα/HeII flux ratios in 11 of

---

[4] This degeneracy disappears when one compares AGN models against models for "normal" HII regions, where the ionizing stellar populations are cooler and result in substantially weaker HeII emission (see, e.g. Feltre et al. 2016; Sobral et al. 2018).
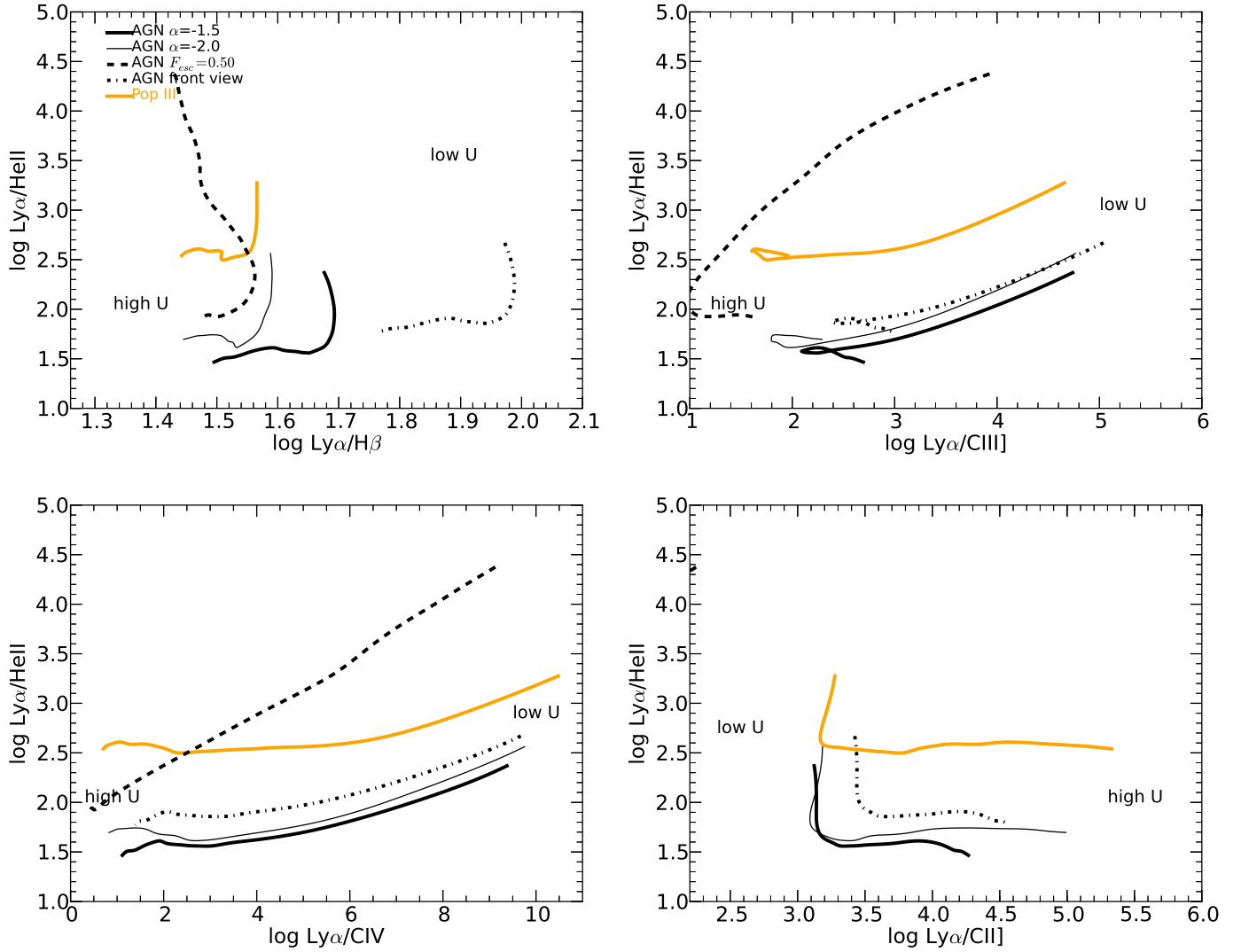
Fig. 7. Diagnostic diagrams comparing Pop III (heavy orange line) and several AGN photoionization models. The AGN model U-sequences shown here are: $\alpha = -1.5$ (thick black line); $\alpha = -2.0$ (thin black line); $\alpha = -1.5$ with "front view" ("back-mirror") (dot-dashed line); photoionization by our $F_{\rm esc}$ filtered AGN continuum (dashed line). All models shown in this figure use $Z/Z_\odot = 0.01$. See main text for further details. The model loci cover the full range of ionization parameter in our model grid, i.e., $-5.55 < \log U < 0.25$.

the 19 halos, typically with higher Lyα/HeII ratios than in high-redshift radio galaxies.

A number of earlier observational studies have also detected extremely high Lyα/HeII flux ratios in extended Lyα-emitting regions around distant AGN, with proposed explanations including enhanced Lyα flux due to the resonance scattering reflection of Lyα by a large-scale unform halo of neutral or possibly matter-bounded gas (see Sect. 3.7), or recombination emission resulting from photoionization of metal-poor gas by the AGN, (e.g. Villar-Martín et al. 2007; Humphrey et al. 2013a; Arrigoni Battaia et al. 2015b).

Our modelling has confirmed that scattering effects can indeed lead to up to a factor of ~2 enhancement of Lyα/HeII, under circumstances that may plausibly be present in the Lyα nebulae of some high-z AGN (see also, e.g. Villar-Martín et al. 1996). However, our models also show that photoionization by an AGN can produce extreme values of Lyα/HeII even without Lyα scattering effects. These include low gas metallicity, a soft or filtered ionizing SED, or a low ionization parameter.

In Fig. 8 we show a selection of relevant photoionization models from our grid, together with the Lyα/HeII flux ratios of

Borisova et al. (2016)[5]. A horizontal line at $\log$ Lyα/HeII = 1.18 delineates the "extreme" and "normal" Lyα/HeII regimes defined in Sect. 2.

Interestingly, all of the ionization models shown in Fig. 8 lie within the "extreme" regime, although at high U the $Z/Z_\odot = 1.0$, $\alpha = -1.5$ curve comes close to the boundary[6]. Thus, we argue that unless $\log U \gtrsim -2.5$ and $Z/Z_\odot \sim 1$, one should expect the intrinsic (emitted) Lyα/HeII ratios of quasar-photoionized halos to be well within the "extreme" regime. We also suggest that for a quasar-ionized halo to appear well inside the "normal" regime ($\log$ Lyα/HeII $\lesssim 1$), its Lyα emission would need to be either strongly absorbed, or else would need to contain a substantial population of matter-bounded clouds that are sufficiently thin for He to be mostly doubly-ionized.

The majority of the quasars in the sample of Borisova et al. (2016) have only lower limits on Lyα/HeII and Lyα/CIV. Unfortunately, these limits are consistent with essentially all of the

---

[5] We have converted the 2σ limits of Borisova et al. (2016) to 3σ.
[6] Our $Z/Z_\odot = 1.0$, $\alpha = -1.0$ curve, not shown in this Figure, just crosses the boundary and reaches down to $\log$ Lyα/HeII = 1.1.
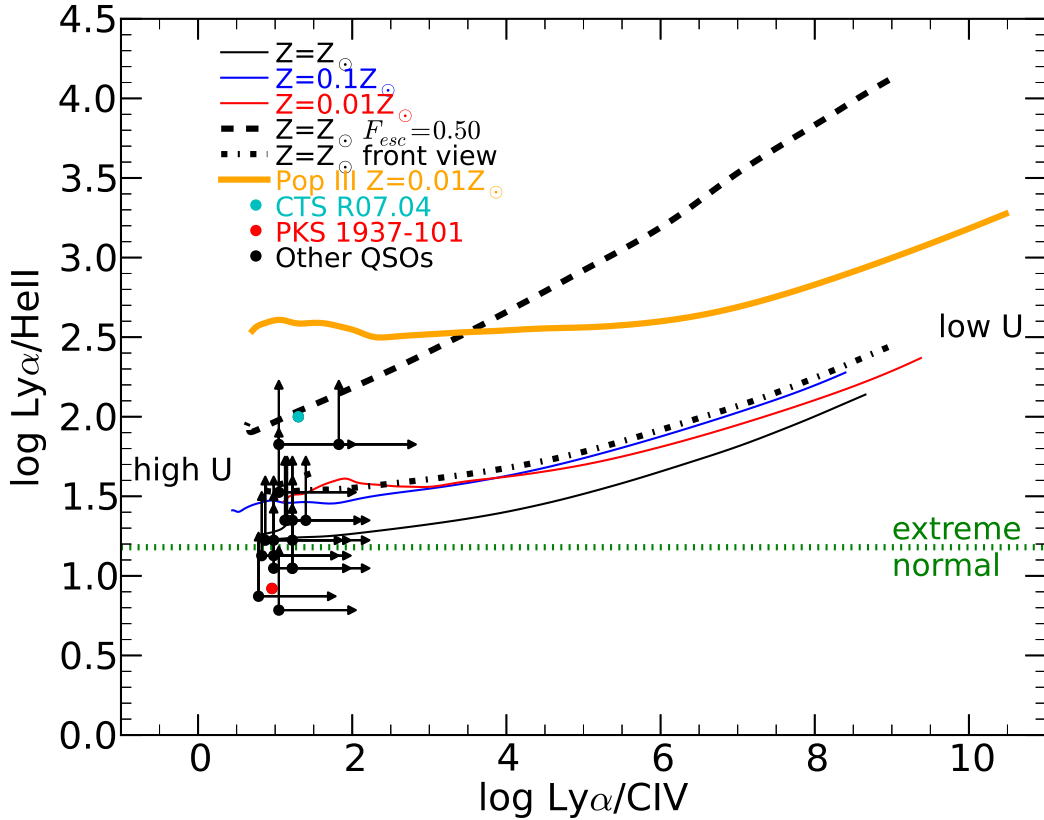
Fig. 8. Lyα/HeII vs. Lyα/CIV showing the locus of several of our photoionization model sequences, along with the measurements or 3σ lower limits on these ratios taken from the Lyα halos of $z \sim 3.5$ quasars of Borisova et al. (2016). The model loci cover the full range of ionization parameter in our model grid, i.e., $-5 < \log U < 0.25$. The horizontal green dotted line marks the boundary between what we define as "extreme" and "normal" Lyα/HeII flux ratios.

models we have considered, and thus we cannot place meaningful constraints on properties such as U, Z, α, etc. for the gas halos of these particular quasars.

Only two quasars in the sample of Borisova et al. (2016) have detections of narrow HeII, and both show large vertical offsets of ~0.3 dex from our AGN powerlaw models. One of these quasars, PKS 1937–101 at $z = 3.77$, shows log Lyα/HeII = 0.92, placing it within the "normal" Lyα/HeII regime in Fig. 8 (red data point). Its position $\gtrsim 0.2$ dex below all of our models (including our $Z/Z_\odot = 1.0$, $\alpha = -1.0$ models) suggests that this quasar halo suffers from strong absorption of Lyα ($N_{HI} \gtrsim 10^{14}$ cm^{-2}), is ionized by an unusually hard SED (i.e., $\alpha < -1.0$), or is composed of matter-bounded clouds rather than the ionization-bounded clouds modelled here.

The other quasar from this sample with a detection of both HeII and CIV is CTS R07.04, at $z = 3.35$ (cyan point in Fig. 8). Its Lyα halo has log Lyα/HeII ~ 2 and log CIV/HeII ~ 5, placing it $\gtrsim 0.4$ dex above our powerlaw AGN model loci, but very close to our $Z/Z_\odot = 1.0$, $F_{esc} = 0.50$ filtered continuum model locus. We suggest that this quasar halo is ionized by an unusually soft SED (for an AGN), due to strong filtering of the quasar's SED by a screen of gas closer to the nucleus, perhaps due to a wide-angle, AGN-driven outflow closer to the nucleus of the galaxy itself. Alternatively, in the case of this quasar one could suppose the presence of a significant contribution from an ionization mechanism that does not produce strong HeII, such as cooling radiation or photoionization by hot, young stars.

With the probable exception of CTS R07.04, we find no need for subsolar gas metallicites, a soft ionizing continuum (including PopIII stars), or enhanced Lyα by scattering to reproduce the

Lyα/HeII flux ratios. However, strictly speaking these are not ruled out.

As a consistency check, we can calculate the Lyα luminosity expected from the implied value of U and the observed size of a Lyα halo, and then compare against observed values of Lyα luminosity from Borisova et al. (2016). For photoionization of gas the expected Lyα luminosity is given by:

$$L_{Ly\alpha} \sim 0.5 \, U \, r^2 \, n_H \, f_c \, \eta_{Ly\alpha} \, \Omega \; (\text{erg s}^{-1}) \quad (1)$$

where f_c is the covering factor of the gas as seen by the ionizing source, n_H (cm^{-3}) is the gas density, U is the ionization parameter, r (cm) is the distance of the cloud from the ionizing source, $\eta_{Ly\alpha}$ is the ratio of emitted Lyα photons to incident ionizing photons (see Sect. 4.2), and Ω is the solid angle (in sr) of the central source covered by the ionized gas[7]. The factor 0.5 arises from the multiplication of the constants 4π, $h\nu_{Ly\alpha}$, c, and $1/4\pi$ sr. Due to the expected uncertainty in the values of n_H, f_c and $\eta_{Ly\alpha}$, we expect uncertainties in resulting estimates of $L_{Ly\alpha}$ to be at least a factor of ~10. Throughout this work, we assume that the ionizing radiation of the AGN is beamed into a bicone covering a solid angle of $\Omega = 3.7$ sr, corresponding to a pair of ionization cones, each with an opening angle of 90°.

Taking one of the most "extreme" cases from Borisova et al. (2016), Q0042–2627 ($z = 3.3$), its Lyα/HeII ratio >67 (1.8 in log) would require log $U \lesssim -4.2$ in our Solar metallicity, $\alpha = -1.5$ powerlaw model sequence, corresponding to $\eta_{Ly\alpha} \sim$

---

[7] The solid angle of an ionization cone with its apex at the position of the central ionizing source is given by $\Omega = 2\pi (1 - \cos \beta)$ sr, where β is the half opening angle of the cone.

0.66 (determined from Fig. 2). Although there is likely to be some radial evolution in one or more of U, n_H, and f_c, the exact behaviour of these parameters in a real halo is far from clear. Thus, we adopt constant but characteristic values for each of them. Adopting $n_H = 100\,cm^{-3}$ and $f_c \sim 0.1$ estimated from radio-loud, type 2 quasars at $z \gtrsim 2$ (e.g. McCarthy 1993; Villar-Martín et al. 2003), assuming $\Omega = 3.7$ sr, and using the maximum observed radius of Lyα emission $r = 4.9 \times 10^{23}$ cm (160 kpc) from Borisova et al. (2016), we estimate $L_{Ly\alpha} \lesssim 1.8 \times 10^{44}$ erg s^{-1} – consistent with the observed luminosity $L_{Ly\alpha} = 1.7 \times 10^{44}$ erg s^{-1} in Table 2 of Borisova et al. (2016). The resulting ionizing luminosity of the AGN would be $Q \lesssim 6 \times 10^{56}$ s^{-1}. The values of $L_{Ly\alpha}$ and Q we have derived are both upper limits because our estimate of U, from which both are derived, is also an upper limit.

Using instead our model sequence with $Z/Z_\odot = 0.1$ and $\alpha = -1.5$, we find $\log U \lesssim -3.8$ and $\eta_{Ly\alpha} \lesssim 1.25$ from Fig. 2. Leaving r, n_H, f_c and Ω unchanged, we obtain $L_{Ly\alpha} \lesssim 9 \times 10^{44}$ erg s^{-1} – still consistent with the observed luminosity. Using the same methodology, we also find a similar level of consistency between the expected and observed $L_{Ly\alpha}$ values for the 10 other quasars from Borisova et al. which show "extreme" Lyα/HeII ratios.

These calculations serve to illustrate the plausibility of very low U, possibly coupled with low gas metallicity, to explain the "extreme" Lyα/HeII ratios measured by Borisova et al. (2016). However, we stress that our consistency check is not intended as proof of a particular value for any of the parameters in Eq. (1).

It seems particularly plausible that the large-scale gas halos of high redshift quasars such as these would have low gas metallicity, since the central galaxy is expected to be fed by cold streams of pristine or very low metallicity gas from the cosmic web (e.g. Goerdt et al. 2015; Vernet et al. 2017). However, observations of the halos of high-z quasars appear to show such halos are already polluted with metals (e.g. Humphrey et al. 2013a; Prochaska et al. 2013).

The detectability of Lyα from extended gas around high-z AGN, and the use of this emission for improving our understanding of galaxy evolution, continue to be key topics in extragalactic astrophysics (e.g. Haiman & Rees 2001; Villar-Martín et al. 2003; Borisova et al. 2016). Our new modelling results have interesting implications for the detectability of Lyα halos associated with high-z AGN. Firstly, cold gas around a quasar should be considerably more luminous in Lyα, and thus easier to detect, if the gas has a lower metallicity and/or if it sees a harder ionizing spectrum. We also suggest that the high detection rate of extended Lyα halos in quasars at high-z (e.g. Borisova et al. 2016) may be due to this effect. In addition, lower gas metallicity and a harder ionizing spectrum could result in apparently larger Lyα halos, as the correspondingly higher $\eta_{Ly\alpha}$ would make faint, outer regions more detectable.

6. Summary

We have used the modelling code MAPPINGS 1e to explore potential mechanisms to produce enhanced Lyα relative to HeII and other emission lines in extended nebulae photoionized by powerful AGN. Our grid of photoionization models cover a substantial range in ionization parameter U, the gas metallicity and the shape of the ionizing continuum, and considers two different electron energy distributions and cloud viewing angles.

We are able to produce "extreme" Lyα/HeII flux ratios using parameters appropriate to extended Lyα emitting halos around high-z quasars. We recover the previously reported Lyα/HeII-

enhancing effects of low metallicity (e.g. Villar-Martín et al. 2007), low U (e.g. Arrigoni Battaia et al. 2015a,b), and cloud perspective (Villar-Martín et al. 1996). Our grid reaches much lower values of U than previous studies by Arrigoni Battaia et al. (2015a,b), and results in even higher values of Lyα/HeII.

As expected from previous studies (e.g. Humphrey et al. 2008; Arrigoni Battaia et al. 2015b), the spectral index of the ionizing powerlaw affects the Lyα/HeII ratio, with a softer spectrum (i.e., $\alpha = -2.0$) resulting in higher Lyα/HeII values. We also find that using a pre-filtered ionizing spectrum can result in extremely high Lyα/HeII ratios, with values reaching as high as $\log$ Lyα/HeII = 4.4 for heavily filtered continua ($F_{esc} = 0.28$) and low ionization parameter ($\log U = -5.55$).

The Lyα/HeII-enhancing effects described above can have a cumulative impact on the Lyα/HeII ratio when two or more of the effects are present in our models. For instance, combining a softer ionizing continuum, a lower gas metallicity and/or low ionization parameter can result in a significantly higher Lyα/HeII ratio than would have otherwise be produced using only one of the above. The most "extreme" model in our grid, which uses $\log U = -5.55$, a heavily filtered continuum ($F_{esc} = 0.28$), low gas metallicity ($Z/Z_\odot = 0.01$) and a maximal contribution from an HI "back-mirror" produces $\log$ Lyα/HeII = 4.6.

In addition to studying the variation of the Lyα/HeII flux ratio, we have also examined the variation in the ratio of emitted Lyα photons to incident ionizing photons, $\eta_{Ly\alpha}$. The value of $\eta_{Ly\alpha}$ ranges from 0.58 to 2.7 in our model grid, deviating substantially from the expected pure-recombination value $\eta_{Ly\alpha} = 0.66$ for optically-thick gas (e.g. Gould & Weinberg 1996). This variation is driven by differences in the electron temperature and H neutral fraction between models, with higher temperature and higher H neutral fraction each resulting in higher rates of collisional excitation of Lyα. In some of our low metallicity models ($Z/Z_\odot = 0.1$) we obtain $\eta_{Ly\alpha} > 1.4$, indicating that collisional excitation is the main channel of Lyα production.

In addition, including the effects of an HI "back-mirror" can increase the observational $\eta_{Ly\alpha}$ by a factor of up to 2, leading to (effective) $\eta_{Ly\alpha}$ values as high as 5.3. Generally speaking, lower gas metallicities, and/or the use of a harder or filtered ionizing SED, results in higher values of $\eta_{Ly\alpha}$. An important implication is that Lyα halos ought to be easier to detect if they have lower gas metallicity or are ionized by a harder or filtered ionizing SED. In principle, this could lead to selection biases in surveys to detect Lyα halos and blobs at high redshift.

Interestingly, we have also found that using κ-distributed electron energies ($\kappa = 20$) instead of Maxwell–Boltzmann-distributed energies can result in slightly enhanced producion of Lyα photons, with a 10–20 percent enhancement in $\eta_{Ly\alpha}$ at high gas metallicity ($Z/Z_\odot = 1.0$ and moderate to low ionization parameter ($\log U \lesssim -2$). However, at low gas metallicity ($Z/Z_\odot \lesssim 0.1$) and high U ($\log U \gtrsim -1.4$) there is a slight ($\sim$10 percent) drop in $\eta_{Ly\alpha}$. A future study will examine in greater detail the impact of κ-distributed electron energies on the emission line spectrum of the narrow line region or Lyα halo of AGN (Morais et al., in prep.).

We have also shown that the extreme Lyα and HeII emission line ratios of the extended Lyα halos of $z \sim 3.5$ quasars studied by Borisova et al. (2016) are consistent with AGN-photoionization of gas with moderate to low metallicity (e.g. $Z/Z_\odot \lesssim 0.1$) and/or low ionization parameter (e.g. $\log U \lesssim -4$), without requiring exotic ionization or excitation mechanisms such as PopIII stars or extreme transfer effects. In the case of the most "Lyα-extreme" quasar from this sample, CTS R07.04 at $z = 3.35$, we find that its Lyα, HeII and CIV flux ratios are

consistent with gas photoionized by a moderately filtered ionizing SED ($F_{esc} \sim 0.5$). We speculate that such filtering may occur in a wide-angle, AGN-driven outflow nearer the nucleus.

Finally, we find that Lyα/HeII alone is insufficient to discriminate between ionization by Pop III stars and an AGN. However, we find that using this ratio together with Lyα/Hβ can provide a clean separation between Pop III and AGN photoionization, even if the gas illuminated by the AGN has very low gas metallicity ($Z/Z_\odot \sim 0.01$).

References

Arrigoni Battaia, F., Yang, Y., Hennawi, J. F., et al. 2015a, ApJ, 804, 26
Arrigoni Battaia, F., Hennawi, J. F., Prochaska, J. X., & Cantalupo, S. 2015b, ApJ, 809, 163
Asplund, M., Grevesse, N., & Jacques Sauval, A. 2006, NuPhA, 777, 1
Binette, L., Dopita, M. A., & Tuohy, I. R. 1985, ApJ, 297, 476
Binette, L., Wang, J., Villar-Martin, M., Martin, P. G., & Magris, C. G. 1993a, ApJ, 414, 535
Binette, L., Wang, J. C. L., Zuo, L., & Magris, C. G. 1993b, AJ, 105, 797
Binette, L., Wilson, A. S., & Storchi-Bergmann, T. 1996, A&A, 312, 365
Binette, L., Groves, B., Villar-Martín, M., Fosbury, R. A. E., & Axon, D. J. 2003, A&A, 405, 975
Binette, L., Matadamas, R., Hägele, G. F., et al. 2012, A&A, 547, A29
Borisova, E., Cantalupo, S., Lilly, S. J., et al. 2016, ApJ, 831, 39
Bowler, R. A. A., McLure, R. J., Dunlop, J. S., et al. 2016, MNRAS, 469, 448
Cantalupo, S., Arrigoni-Battaia, F., Prochaska, J. X., Hennawi, J. F., & Madau, P. 2014, Nature, 506, 63
De Breuck, C., Röttgering, H., Miley, G., van Breugel, W., & Best, P. 2000, A&A, 362, 519
Dors, O. L., Agarwal, B., Hägele, G. F., et al. 2018, MNRAS, 479, 2294
Draine, B. T., & Kreisch, C. D. 2018, ApJ, 862, 30
Ferland, G. J., Henney, W. J., O'Dell, C. R., & Peimbert, M. 2016, Rev. Mex. Astron. Astrof., 52, 261
Feltre, A., Charlot, S., & Gutkin, J. 2016, MNRAS, 456, 3354
Ferruit, P., Binette, L., Sutherland, R. S., & Pecontal, E. 1997, A&A, 322, 73
Fosbury, R. A. E., Villar-Martín, M., Humphrey, A., et al. 2003, ApJ, 596, 797
Francis, P. J. 1993, ApJ, 407, 519
Goerdt, T., Ceverino, D., Dekel, A., & Teyssier, R. 2015, MNRAS, 454, 637
Gould, A., & Weinberg, D. H. 1996, ApJ, 468, 462
Haiman, Z., & Rees, M. J. 2001, ApJ, 556, 87
Heckman, T. M., Lehnert, M. D., Miley, G. K., & van Breugel, W. 1991, ApJ, 381, 373
Holden, B. P., Stanford, S. A., Squires, G. K., et al. 2001, AJ, 122, 629
Humphrey, A., & Binette, L. 2014, MNRAS, 442, 753
Humphrey, A., Villar-Martín, M., Vernet, J., et al. 2008, MNRAS, 383, 11
Humphrey, A., Vernet, J., Villar-Martín, M., et al. 2013a, ApJ, 768, L3
Humphrey, A., Binette, L., Villar-Martín, M., Aretxaga, I., & Papaderos, P. 2013b, MNRAS, 428, 563
Husemann, B., Worseck, G., Arrigoni Battaia, F., & Shanks, T. 2018, A&A, 610, L7
Livadiotis, G. 2018, Europhys. Lett., 122, 5
Livadiotis, G., & McComas, D. J. 2011, ApJ, 741, 88
McCarthy, P. J. 1993, ARA&A, 31, 639
Nicholls, D. C., Dopita, M. A., & Sutherland, R. S. 2012, ApJ, 752, 148
Nicholls, D. C., Dopita, M. A., Sutherland, R. S., Kewley, L. J., & Palay, E. 2013, ApJS, 207, 21
Prochaska, J. X., Hennawi, J. F., & Simcoe, R. A. 2013, ApJ, 762, L19
Robinson, A., Binette, L., Fosbury, R. A. E., & Tadhunter, C. N. 1987, MNRAS, 227, 97
Rosdahl, J., & Blaizot, J. 2012, MNRAS, 423, 344
Schaerer, D. 2002, A&A, 382, 28
Shibuya, T., Ouchi, M., Konno, A., et al. 2018, PASJ, 70, S14
Shull, J. M., Stevans, M., & Danforth, C. W. 2012, ApJ, 752, 162
Sobral, D., Matthee, J., Darvish, B., et al. 2015, ApJ, 808, 139
Sobral, D., Matthee, J., Darvish, B., et al. 2018, MNRAS, 477, 2817
Sobral, D., Matthee, J., Brammer, G., et al. 2019, MNRAS, 482, 2422
Stevans, M. L., Shull, J. M., Danforth, C. W., & Tilton, E. M. 2014, ApJ, 794, 75
Taniguchi, Y., Trentham, N., Ikeuchi, S., et al. 2001, ApJ, 559, L9
Telfer, R. C., Zheng, W., Kriss, G. A., & Davidsen, A. F. 2002, ApJ, 565, 773
Tenorio-Tagle, G., Silich, S. A., Kunth, D., Terlevich, E., & Terlevich, R. 1999, MNRAS, 309, 332
van Ojik, R., Rottgering, H. J. A., Miley, G. K., et al. 1994, A&A, 289, 54
Vasyliunas, V. M. 1968, ASSL, 10, 622
Vernet, J., Fosbury, R. A. E., Villar-Martín, M., et al. 2001, A&A, 366, 7
Vernet, J., Lehnert, M. D., De Breuck, C., et al. 2017, A&A, 602, L6
Villar-Martín, M., Binette, L., & Fosbury, R. A. E. 1996, A&A, 312, 751
Villar-Martín, M., Tadhunter, C., & Clark, N. 1997, A&A, 323, 21
Villar-Martín, M., Vernet, J., di Serego Alighieri, S., et al. 2003, MNRAS, 346, 273
Villar-Martín, M., Cerviño, M., & González Delgado, R. M. 2004, MNRAS, 355, 1132
Villar-Martín, M., Humphrey, A., De Breuck, C., et al. 2007, MNRAS, 375, 1299

Appendix A: Alternate version of Fig. 5

Here we show an alternate version of Fig. 5, showing the same model loci, but plotted as a function of $U_* = U/F_{esc}$ to aid comparison with our unfiltered models.
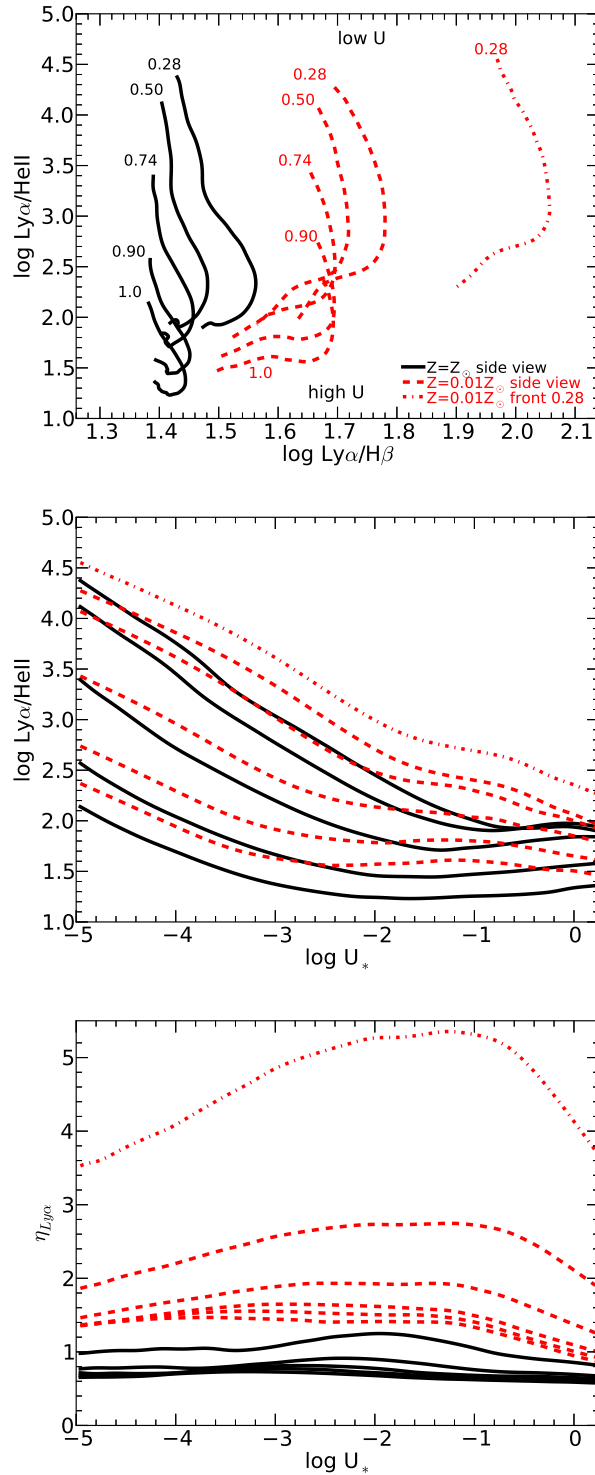

Fig. A.1. Impact of using a filtered ionizing continuum instead of a simple powerlaw on the observed values of Lyα/HeII, Lyα/Hβ and $\eta_{Ly\alpha}$. In order that the curves be aligned, the models are plotted as a function of log U_* where $U_* = U/F_{esc}$. In the *upper panel*, the U_*-sequences using a filtered ionizing continuum are labelled with their respective value of F_{esc}. U_*-sequence loci which use our default powerlaw of $\alpha = -1.5$ are labelled "1.0" because the input SED is unfiltered. The dot-dashed curve (on the right of the *upper panel*) shows the locus of our sequence in U_* that uses $F_{esc} = 0.28$, $Z/Z_\odot = 0.01$, $\alpha = -1.5$ and the "front view", to illustrate the combined effect of low U_*, low gas metallicity, a heavily filtered ionizing continuum, and a "back-mirror". For each combination of U_* and $Z/Z_\odot$, a lower F_{esc} results in a lower Lyα/HeII.